Marine Pollution Bulletin 196 (2023) 115568

Contents lists available at ScienceDirect

Marine Pollution Bulletin

journal homepage: www.elsevier.com/locate/marpolbul

Occurrence, characteristics, and factors influencing the atmospheric microplastics around Jiaozhou Bay, the Yellow Sea

Chenhao Zhao [a,d], Junhua Liang [a,b], Mingliang Zhu [a,b], Shan Zheng [a,b], Yongfang Zhao [a,b], Xiaoxia Sun [a,b,c,d,*]

[a] Jiaozhou Bay National Marine Ecosystem Research Station, Institute of Oceanology, Chinese Academy of Sciences, Qingdao 266071, PR China
[b] Laboratory for Marine Ecology and Environmental Science, Laoshan Laboratory, 266237, PR China
[c] Center for Ocean Mega-Science, Institute of Oceanology, Chinese Academy of Sciences, Qingdao 266071, China
[d] University of Chinese Academy of Sciences, Beijing 100049, China

ARTICLE INFO

Keywords:
Atmospheric fallout
Air-sea interaction
Seasonal variation
Monsoons
Rainy season

ABSTRACT

Atmospheric microplastics are attracting increasing attention as an emerging pollutant. However, research on its characteristics and influencing factors is insufficient. This study examines the characteristics and spatiotemporal distribution of atmospheric microplastics around Jiaozhou Bay, the Yellow Sea. The results showed that the dominant shapes of microplastic were fragments (61.9 %) and fibers (25.6 %), and the main types were polyethylene terephthalate (23.8 %), polyethylene (31.6 %) and cellulose (rayon, 34.9 %). The deposition rate of microplastic varied from 8.395 to 80.114 items·m^{-2}·d^{-1}, with a mean of 46.708 ± 21.316 items·m^{-2}·d^{-1}. The deposition rate was higher in the dry season than in the rainy season, indicating the influence of weather condition. The annual mass of atmospheric microplastics entering the bay was estimated to be 7.612 ± 3.474 tons. For the first time, this study reveals that atmospheric microplastics in Jiaozhou Bay change spatiotemporally due to monsoons, which pose a potential threat to marine ecosystems.

1. Introduction

Microplastics (MPs) are generally defined as synthetic materials with characteristic lengths of <5 mm (Andrady, 2011; Cole et al., 2011). MPs can be divided into primary MPs and secondary MPs according to their source. Generally, primary MPs are manufactured in small sizes and granule shapes, and mainly sourced from commercial products such as personal care, cosmetics, and medical products. Secondary MPs originate from the cracking and degradation of larger plastics through physical, chemical, and biological processes, with varied shapes (fibers, fragments, and films) (Fendall and Sewell, 2009; O'Brine and Thompson, 2010). In the past decade, MPs have gained considerable attention from the public, academia, and government agencies as an emerging pollutant (Hüffer et al., 2017), which necessitates comprehensive research on MPs' occurrence, fate, and effects.

Research on MPs began in the oceans and then developed into terrestrial and the biosphere. From the Antarctic to the Arctic, the researchers found that MPs are ubiquitous in almost every ecosystem (Rochman, 2018; Xu et al., 2022), as well as in multiple species (Ding et al., 2020; Wang et al., 2019). Furthermore, it has been established that the ingestion of MPs causes physical injury and inflammatory responses in organisms (de Sá et al., 2018; Xuan et al., 2023). Humans can ingest and inhale MPs, leading to their accumulation in several organs and tissues, such as the blood, liver, lung, placenta, kidney, spleen (Rahman et al., 2021), and causing several detrimental effects, such as secondary genotoxicity and immune responses (Kutralam-Muniasamy et al., 2023b; Pironti et al., 2021; Xuan et al., 2023). Additionally, both additives (plasticizers, dyes, flame retardants, and stabilizers) in plastic production and surface attachments (polycyclic aromatic hydrocarbons (PAHs), polychlorinated biphenyls (PCBs), and heavy metals) absorbed to aged MPs increase the toxicity of MPs, posing greater potential threats to organisms and ecological environment (Guo and Wang, 2021; Hahladakis et al., 2018; Pastorino et al., 2021).

Atmospheric microplastics (AMPs) research began comparatively later than research on MPs in soil, water bodies and organisms, with the first monitoring taking place in Paris by Dris et al. (2015). Subsequently, high concentrations of AMPs were commonly observed in diverse environments, such as urban areas (Jia et al., 2022; Liu et al., 2022),

* Corresponding author at: 7 Nanhai Road, Qingdao 266071, China.
E-mail address: xsun@qdio.ac.cn (X. Sun).

https://doi.org/10.1016/j.marpolbul.2023.115568
Received 26 July 2023; Received in revised form 11 September 2023; Accepted 19 September 2023
Available online 30 September 2023

suburban and mountain regions (Bergmann et al., 2019; Truong et al., 2021), inshore areas and oceans (Ferrero et al., 2022; Wang et al., 2022). AMPs abundance is generally higher in cities than in suburban areas due to their proximity to MPs' sources (Truong et al., 2021). Existing studies believed that AMPs come from synthetic textile emissions, wear of rubber tires, degradation of plastics and resuspension of dust (Evangeliou et al., 2020; Wright et al., 2020). Meanwhile, studies confirmed that AMPs can travel long distances and even enter the free troposphere (Allen et al., 2021), thereby increasing the exposure risk of remote areas by atmospheric deposition and the interception of forests (Huang et al., 2022; Klein and Fischer, 2019). The transport process of AMPs is affected by circulation, precipitation, and atmospheric dynamics (Ferrero et al., 2022; Jia et al., 2022). Given that AMPs can be directly inhaled by humans through respiration and accumulate in the lungs, they may pose a greater threat to human health than MPs in water and soil (Kutralam-Muniasamy et al., 2023a).

Recent researches have attempted to quantify the transport of MPs between atmosphere and other environmental media by constructing models. The resulting simulations, however, are characterized by a high degree of uncertainty, which may be attributed to an inadequate amount of data (Allen et al., 2022; Long et al., 2022). At present, the study of AMPs deposition in coastal regions has proven insufficient to accurately reflect the features of global AMPs deposition into the ocean (Allen et al., 2022). Consequently, it is imperative to enrich the data of AMPs deposition. In addition, the abundance and distribution of AMPs are influenced by a variety of anthropogenic and natural factors. The analysis of these factors helps to understand the sources of AMPs and reduce AMP pollution.

This study endeavored to investigate the deposition characteristics of AMPs in Jiaozhou Bay, located in Shandong Province, China and connecting to the Yellow Sea, under a temperate monsoonal climatic over the course of a year. The presence of a large population, developed economy and abundant industries surrounding Jiaozhou Bay, and the prevalence of research regarding MPs in water, biology, and sediment within this area, make Jiaozhou Bay an ideal research object. Therefore, this study aims to: (i) investigate the abundance and characteristics of AMPs in the coastal area; (ii) analyze the relationship between AMPs and MPs in other environmental media; and (iii) determine the influence of various factors on AMPs. The results of this study are expected to enhance our knowledge of AMPs deposition in offshore and bays, deepen the understanding of AMPs as an important pathway for MPs to enter the sea, and shape the development of more accurate MPs cycle models in the future.

2. Methods

2.1. Study area

Jiaozhou Bay is a semi-enclosed bay located in the middle of the Yellow Sea in China, with an area of approximately 444 km^2 (Li et al., 2020). Qingdao, a big city distributed around Jiaozhou Bay, own a resident population of 9,499,800 and a regional Gross Domestic Product (GDP) of 1174.131 billion yuan (173.771 billion dollars) in 2019 (Qingdao Municipal Statistics Bureau, 2020). According to the analysis of geographical environment, population distribution and industrial distribution, five sampling sites were selected. These sites are in five administrative districts of Qingdao, and are evenly spaced around Jiaozhou Bay. Site S1 is located on the north of Jiaozhou Bay, belonging to Chengyang District. To the east of site S1 is mariculture ponds, and to the west is a theme park. Site S2 was set up on a dam on the northwest of the Bay, with a large area of vegetation in the north and the sea surface in the other directions. Site S3 stands in a commercial port on the east of Jiaozhou Bay, belonging to the Shibei District. Its north is the passenger transport center, and the south is the harbor basin and residential area. Site S4 is in a meteorological station on the southeast of Jiaozhou Bay, belonging to the Shinan District. It has construction sites on the north and is surrounded by the sea in the other directions. Site S5 belongs to Huangdao District, located in an industrial port on the southwest side of Jiaozhou Bay, adjacent to the residential area to the south and west direction, and the shipyard to the north side. The characteristics of the sampling sites are shown in Fig. 1 and Table 1.

2.2. Sampling collection

AMPs samples were continuously collected from December 2018 to December 2019 by passive sampling method at five selected sampling sites over four quarters: quarter Q1 (Winter, December 5–March 3, 89 days), quarter Q2 (Spring, March 4–June 3, 92 days), quarter Q3 (Summer, June 4–September 2, 91 days) and quarter Q4 (Autumn, September 3–December 4, 93 days). It was ensured that the sampling started and finished at the same time of one day.

According to a method of Zhou et al. (2017) with a slight modification, a glass bottle with a volume of 5 L was used as the sampling container, and a glass funnel with an inner diameter of 10 cm was used as the collector. The sampling container and the collector were connected by an intermediate segment, as shown in Fig. S1. The collector is designed as a funnel type to avoid secondary suspension of the sample and wind interference. All collection devices were flushed with pre-filtered distilled water several times before use and dried in a clean enclosed space to avoid introducing additional contamination. At the end of one phase of sampling, the glass funnel was rinsed with 300 mL pre-filtered ultrapure water for three times, and then the rinsed liquid was transferred to the 5 L sampling bottle. The sampling bottle was sealed, transported to the laboratory, and stored in a 4 °C refrigerator until use. The newly cleaned glass bottle was installed below the funnel to start the next phase of sampling.

2.3. Laboratory procedures

Refer to the previous research and modify it appropriately to pretreat AMPs (Dris et al., 2016; Zhou et al., 2017). All the distilled water and 10 % potassium hydroxide (KOH) solution used in this research were pre-filtered by glass microfiber filter (pore size 1.2 μm, Ø47 mm, GF/C 1822–047, Whatman PLC., UK). Firstly, the liquid in the glass bottle was poured into a stainless-steel sieve (Standard sample sieve, Jiufeng, China) of 900 mesh (sieve pore diameter is approximately 15 μm) for reducing sample volume by filtration. The glass bottle was rinsed with distilled water for 3 times, and the rinsed liquid was also passed through the sieve. Once filtration was completed, the residual sample on the sieve was transferred to a 250 mL flask.

The digestion process was carried out by adding 10 % KOH solution to the flask and then heating with water bath. 200 mL 10 % KOH solution was added to each flask, and then the flasks were heated at 60 °C by an electric shaker (SHA-BA, Danrui Ltd., China) for 24 h. Subsequently, the sample in the flask was filtered with glass microfiber filter (pore size 1.2 μm, Ø47 mm, GF/C 1822–047, Whatman PLC., UK). The inner wall of the flask was rinsed with distilled water three times, and the rinsed liquid was similarly filtered with the same filter. After filtration, the filtration membrane was stored in a clean petri dish, and saved in a 4 °C refrigerator until the next process.

MPs were initially identified using a microscope (SteREO Discovery. V8, Carl Zeiss Microscopy GmbH., Germany), and suspected MPs were selected based on hardness test and some criteria confirmed by previous study (particle size <5 mm, homogeneous and unnatural colour, no shape like cell tissue, and no branches or segments) (Suteja et al., 2021). Suspected MPs were classified according to their shape and colour. The size of suspected MPs was measured under the microscope by matching software (ZEN2.3 blue edition, Carl Zeiss Microscopy GmbH., Germany). A subset (1/4) of suspected MPs was randomly selected and identified using a Fourier transform infrared spectrometer (FTIR; Spotlight 400, Perkin Elmer Inc., USA) in ATR (attenuated total reflectance) mode. The instrument parameters of FTIR were set as follows: scanning

Fig. 1. The sampling sites of AMPs in Jiaozhou Bay. The red dots in the large figure represent the location of the sampling sites, and the red box in the small figure at the lower left represents the position of Jiaozhou Bay relative to the surrounding sea and land. (For interpretation of the references to colour in this figure legend, the reader is referred to the web version of this article.)

Table 1
Characteristics of the sampling sites.

Sampling sites	Functional status	Longitude (E)	Latitude (N)	Distance from the coastline (m)	Height (m)
S1	Cultural area	120.283647	36.211125	134.5	2.5
S2	Wetland reserve	120.128242	36.155275	0.7	6.1
S3	Commercial port	120.310931	36.083481	2.2	1.2
S4	Residential area	120.290600	36.044622	56.4	1.1
S5	Industrial port	120.240636	35.979478	18.9	10.5

range from 750 to 4000 cm^{-1}, scanning times 32, pixel size 6.25 μm, and sampling size 400 μm × 400 μm. The resulting spectra were compared with the standard plastic spectra in standard spectra library (Sadtler FTIR Library), with the chemical type being deemed equal when the similarity exceeded 70 %. Pre-filtered ultrapure water was used as a blank group and the steps in Section 2.3 were repeated. No MPs were detected in the blank samples.

2.4. Meteorological data and urban data

The meteorological data for the Qingdao 54,857 Meteorological Station (120° 20′ E, 36° 04′ N) was obtained from the rp5.ru website (https://rp5.ru/Weather_in_the_world) (Raspisaniye Pogodi Ltd., 2023). The daily meteorological data during the sampling period was calculated to monthly data and the four sampling quarters were classified into rainy season (Q2 and Q3 quarter, 183 days, 428.4 mm total rainfall) and dry season (Q1 and Q4 quarter, 182 days, 65.6 mm total rainfall) according to the total rainfall. The backward trajectory analysis of atmospheric motion was performed using the Hysplit model (web version) (https://www.ready.noaa.gov/hypub-bin/trajtype.pl?runtype=archive) (National Oceanic and Atmospheric Administration, USA). The GDAS (1°, global, 2006-present) meteorological dataset was selected for 24 h of backward trajectory analysis at 10 m, 100 m and 500 m altitudes, respectively. Additionally, information regarding population density, GDP, industrial production, and other data related to the districts in Qingdao jurisdiction was extracted from the 2020 Qingdao Statistical Yearbook (Qingdao Municipal Statistics Bureau, 2020).

2.5. Data calculation and statistical analysis

Deposition rate (D) was used to measure the abundance of AMPs. The unit of the deposition rate is items·m^{-2}·d^{-1}, which means the number of AMPs collected per square meter of sampling area per day. The specific calculation method is shown in Eq. (1):

$$D = \frac{n}{s \times t} \tag{1}$$

In this equation, n is the number of MPs in a single sample (items), s is the opening area of the sampling container (m^2), and t is the total sampling time (day).

The volume and weight of MPs were estimated with their size and shape according to the method proposed by Zheng et al. (2020). The mass of different MPs was obtained through multiplying their density by their volume.

$$V_f = \pi r^2 h \tag{2}$$

$$V_n = 4/\pi r^3 \alpha \tag{3}$$

$$W = V_f(V_n) \times \rho \tag{4}$$

V_f and V_n represent the volume of fibers and non-fibers MPs respectively, and W represents the weight of MPs. Where r is the radius of fibers or non-fibers (for non-fibers, r is the geometric mean of the half of the length and width), h is the length of the fibers, ρ is the density of different MPs, and α is the shape factor (for fragment and film, $\alpha = 0.1$; for granule and foam, $\alpha = 1$).

Statistical analysis was executed using Origin Pro 2022 and the

statistical package for the social sciences (SPSS). Mann-Whitney *U* test, Pearson Chi-Square test, Fisher's Exact Test and Kruskal-Wallis test were performed to analyze the spatiotemporal changes of deposition rate and characteristics of AMPs with a significance level (p) at 0.05.

2.6. Quality control

To ensure that the experiment is not interfered by external factors, stringent quality control measures were adopted: (i) Pure cotton test suits were worn throughout the laboratory process; (ii) All liquid reagents were pre-filtered prior to use; (iii) All containers were washed three times with pre-filtered distilled water before use. The sample was covered with glass cover or aluminum foil before and after the experiment; (iv) Each equipment and worktable in the laboratory was cleaned with pre-filtered 70 % ethanol before the experiment; (v) Air flow was limited by restricting the movement of people and closing windows of the laboratory; (vi) Usage of any plastic apparatus or equipment was avoided; and (vii) pre-filtered distilled water was used as blank samples in laboratory procedures.

3. Results and discussion

3.1. The characteristics of AMPs

3.1.1. Shapes of AMPs

A detailed analysis of the shapes of the deposited AMPs in Jiaozhou Bay revealed the dominance of fragments, fibers, and granules, with percentages of 61.9 %, 25.6 % and 10.5 %, respectively (Fig. 2a). Fragmented MPs were the most prevalent in all sampling quarters, with higher percentages in quarters Q2 and Q3 than in quarters Q1 and Q4 (Fig. 2b). Conversely, the proportion of fibrous MPs in quarters Q1 and Q4 was higher than that in quarters Q2 and Q3. There was a significant difference in the percentage of shapes between different sampling quarters (Fisher's Exact Test, $p < 0.05$), which suggests variations in environmental factors affecting MPs generation and diffusion. Additionally, fragmented MPs were the most abundant across all sampling sites (Fig. 2c), and there was a notable difference in the percentage of shape between different sampling sites (Fisher's Exact Test, $p < 0.05$). Significant variation in the percentage of MPs shape was also observed between the dry and rainy seasons (Fisher's Exact Test, $p < 0.05$). Specifically, the deposited AMPs observed during the rainy season showed a higher percentage of fragmented MPs and fewer fibrous MPs relative to the dry season (Fig. 2d).

Pervious research indicated that urban deposited AMPs predominantly have a fiber-based shape, such as in Dongguan-China (90.11 %),

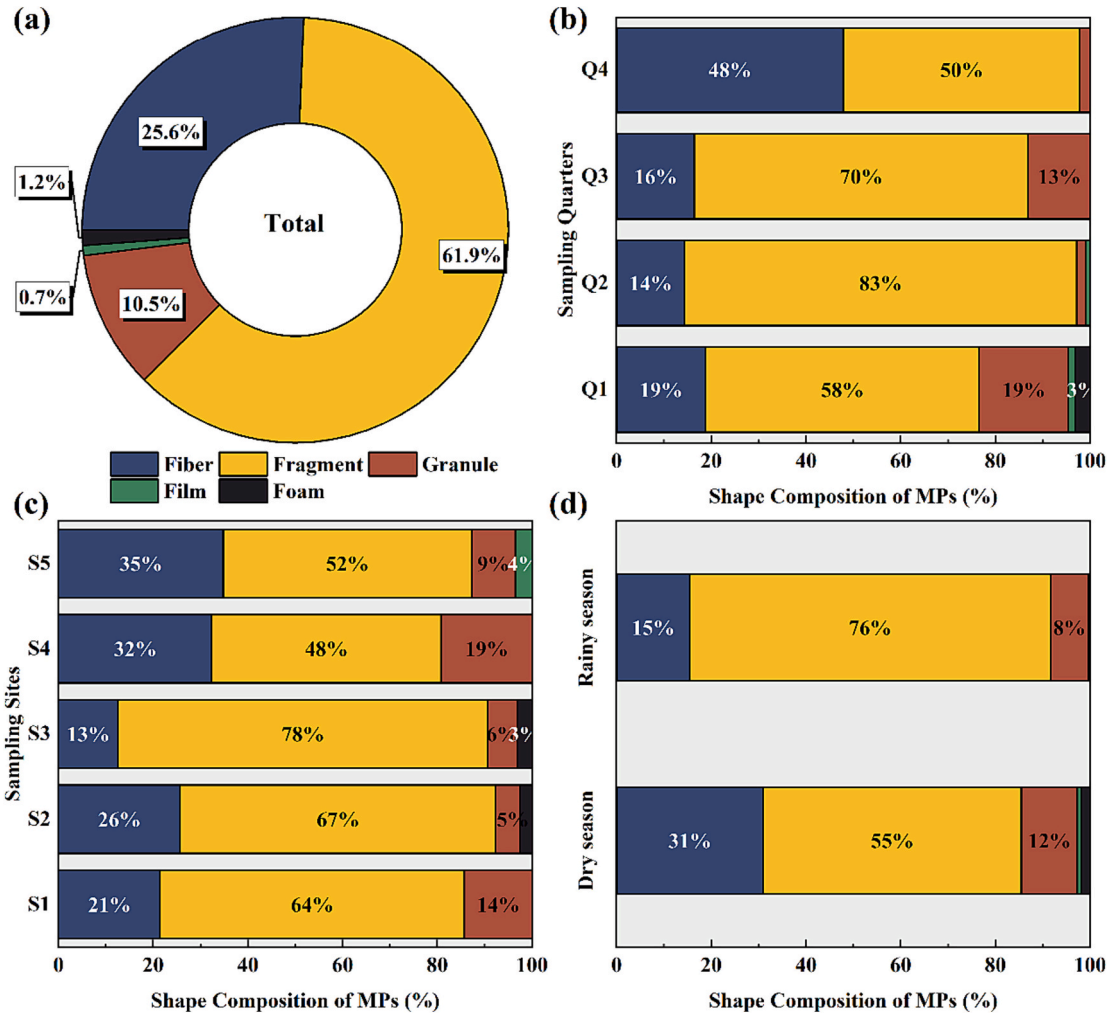

Fig. 2. The percentage of AMPs shape in Jiaozhou Bay. (a) The percentage of all AMPs shapes. (b) The percentage of AMPs shapes in different quarters. (c) The percentage of AMPs shapes in different sampling sites. (d) The percentage of AMPs shapes in dry and rainy seasons.

London-United Kingdom (92 %), and Jakarta-Indonesia (86.36 %) (Cai et al., 2017; Purwiyanto et al., 2022; Wright et al., 2020). Mbachu et al. (2020) suggested that the prevalence of fibrous MPs is attributed to their smaller mass-to-area ratio compared with other MPs, thus facilitating their diffusion and resuspension. In addition, the clothing industry and laundry activities in urban population gathering areas provide a rich source of fibrous MPs as polymer fibers can fall off from textiles and then suspend into the atmosphere (Xu et al., 2022).

Fragmented MPs, however, were dominant in some cities, such as Hamburg-Germany (95 %), Kathmandu-Nepal (71.3 %), and Beijing-China (70.9 %) (Klein and Fischer, 2019; Liu et al., 2022; Yukioka et al., 2020). One potential explanation for such a discrepancy lies in the difference in MPs production in different regions. Specifically, fiber-based MPs are generally derived from the textile industry and household textile washing, while fragmented MPs result from the degradation of primary plastic products (Xu et al., 2022). Therefore, urban areas with unique industrial structures and population densities are likely to exhibit different MPs composition. Furthermore, the climate conditions have additional influence on the production and spread of MPs. Generally, fragmented MPs are generated from the disintegration of larger particles by mechanical wear and exposure to ultraviolet light (Bonifazi et al., 2023; Wang et al., 2023), thus increased temperatures and extended sunshine duration are expected to cause higher production of fragmented MPs. Fibrous MPs, however, are more prone to wind-driven transport (Bullard et al., 2021), which increases the possibility of them to be diffused and resuspended in the windy seasons. The impact of environmental factors on MPs morphology is further evidenced by the variations in MP shapes observed across different sampling sites in this experiment. Notably, site S5 features a significantly greater sampling height in comparison to other sites, and thus receives more fibrous MPs transported by wind, resulting in the highest proportion of fiber shapes among all sites.

Investigations into the shape composition of MPs in various environmental media in Jiaozhou Bay have yielded inconsistent results. Zheng et al. (2020) highlighted that MPs in the sediments of Jiaozhou Bay were generally composed of polymeric fibers (70.6 %–90.4 %), while Liu et al. (2020b) depicted the high prevalence of fragmented MPs (52 %) in surface seawater. It is speculated that AMPs of Jiaozhou Bay stem primarily from Qingdao and nearby urban areas, largely influenced by climatic conditions and deposited into the surface seawater. However, the shape composition of MPs in the water and sediments of the whole Jiaozhou Bay depends on more factors, such as runoff input of

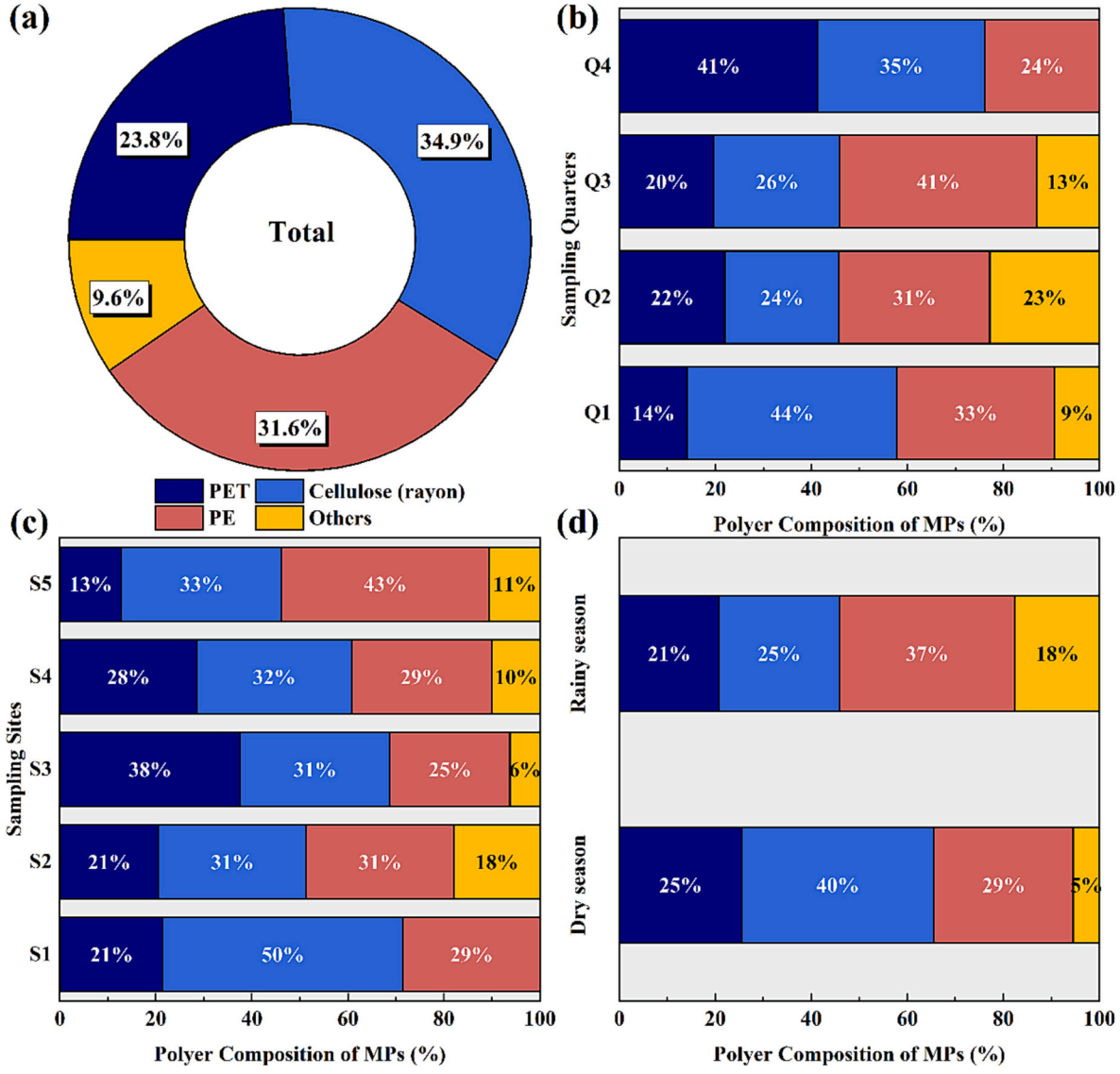

Fig. 3. The percentage of AMPs types in Jiaozhou Bay. (a) The percentage of all AMPs types. (b) The percentage of AMPs types in different quarters. (c) The percentage of AMPs types in different sampling sites. (d) The percentage of AMPs types in dry and rainy seasons.

MPs and biological disturbance in water and sediments (Jiao et al., 2022; Ouyang et al., 2020; Zhang et al., 2023).

3.1.2. Chemical types of AMPs

We identified 14 types of MPs using FTIR in the selected samples. Cellulose (rayon), polyethylene (PE) and polyethylene terephthalate (PET) were the most abundant, accounting for 34.9 %, 31.6 % and 23.8 % of the total MPs, respectively (Fig. 3a). The remaining MPs included polyamide (PA), polypropylene (PP), poly (1,4-cyclohexanedimethylene terephthalate) (PCT), polyoxymethylene (POM) and polyvinyl fluoride (PVF), which were grouped as "others" due to their low percentages (9.6 % of the total MPs). Among these MPs, PA, POM and PP were the most prevalent, with 1.8 %, 1.65 % and 1.2 % of the total MPs, respectively. The chemical types of MPs varied significantly by sampling quarters and sites (Pearson Chi-Square test, $p < 0.05$) (Fig. 3b and c). For instance, cellulose (rayon) was the dominant type in quarter Q1, PE in quarters Q2 and Q3, and PET in quarter Q4. Similarly, PE, PET, and cellulose (rayon) were the predominant types of AMPs at sites S5, S3 and S1, respectively. Notably, we observed a significant difference in chemical types of MPs between rainy and dry seasons (Pearson Chi-Square test, $p < 0.05$) (Fig. 3d). PE MPs had a higher proportion in the rainy season than in the dry season, whereas PET and cellulose (rayon) were less prevalent in the rainy season than in the dry season.

PET is a common polymer that is synthesized by polycondensation of terephthalic acid and ethylene glycol. PET has been widely used in the production of polyester fibers and various textile products. Moreover, PET exhibits good corrosion resistance, insulation, heat resistance, and flexibility, which make it suitable for plastic films, bottles, and engineering plastics (Ratner, 2012). PE is another common polymer that is obtained by polymerization of ethylene monomer. PE has excellent insulation, corrosion resistance, and stable physical properties, which enable its use in pipes, plates, films, and high-strength fibers (Dhakal and Ismail, 2021). Cellulose (rayon) is a chemical fiber made from natural polymers through chemical and mechanical processing. Cellulose (rayon) is classified as an artificial fiber because it contains industrial additives such as dyes, flame retardants, and light stabilizers in its raw materials. It is mainly used for the manufacture of textile and apparel (Chen, 2015).

The presence and dominance of PET, PE, and cellulose in urban AMPs has also been found in other cities such as Dongguan (cellulose 73 %, PE 14 %, PP 9 %, PS 4 %), Jakarta (PET 81.82 %, PE 7.58 %, PB 7.58 %, PS 3.03 %), and Mexico (cellophane 67.5 %, PE 12.5 %, PET 8.75 %, cellulose 7.5 %) (Cai et al., 2017; Purwiyanto et al., 2022; Shruti et al., 2022). China is a major producer and consumer of PET and PE plastics. In 2017, China produced 41.1 million tons of PET and 14.72 million tons of PE, but only recycled and treated 79.5 % of PE and PET in waste plastics (Chu et al., 2023). Qingdao, a leading industrial city in northern China, had 281 textiles, clothing, and chemical fiber manufacturing enterprises and 268 rubber and plastic manufacturing enterprises in 2019, which constituted 7.95 % and 7.58 % of Qingdao's total industrial enterprises, respectively. In the same year, Qingdao generated a total of 644,700 tons of plastic products and 39,100 tons of chemical fibers (Qingdao Municipal Statistics Bureau, 2020). The developed industrial production and the accumulation of plastic waste may provide a local source of AMPs in Jiaozhou Bay to some extent.

The chemical types and proportions of MPs found in water, sediments, and aquatic organisms within Jiaozhou Bay are comparable to that found in AMPs, but with some notable differences. Specifically, PET, PE, or rayon were the most abundant types in estuarine water (with PET comprising 78.57 % and PE 10.72 %), estuarine sediments (with PET at 43.37 % and PE and rayon each at 21.74 %), seabed sediments (with PET and rayon together at 62.2 %), and benthic fauna (with PE at 62.4 %, PET at 11.4 %, and rayon at 14.9 %) (Zhang et al., 2023; Zheng et al., 2020; Zheng et al., 2019). Nevertheless, the proportion of rayon was significantly lower than that of AMPs in this study (with rayon at 34.9 %, PE at 31.6 %, and PET at 23.8 %). We suggest that variations in the source and influence of MPs across different environmental media, as well as MPs' shape, size, and density, may contribute to their differential distribution.

3.1.3. Size of AMPs

The size of AMPs in Jiaozhou Bay ranged from 31.96 to 3407.546 μm, with a mean of 331.507 ± 517.323 μm. The MPs were classified into six categories based on their sizes: 0–100 μm, 100–200 μm, 200–500 μm, 500–1000 μm, 1000–2000 μm, and 2000–5000 μm. As shown in Fig. 4a, the relative abundance of AMPs decreased as the size increased. The smallest size category (0–100 μm) accounted for the highest proportion of AMPs (33.1 %). The size distribution of AMPs varied significantly across quarters Q1 to Q4 (Pearson Chi-Square test, $p < 0.05$) (Fig. 4b). All MPs in quarter Q3 were smaller than 1000 μm, and their proportion (100 %) was significantly higher than in other quarters. In contrast, quarter Q4 had the highest proportion of MPs larger than 100 μm (87 %), which was significantly different from other quarters. The size distribution of AMPs also differed significantly among sites (Pearson Chi-Square test, $p < 0.05$) (Fig. 4c). Sites S1 and S2 in the northern part of Jiaozhou Bay had similar proportions of MPs smaller than 200 μm (75 % and 70 %, respectively) to site S3 in the central part of Jiaozhou Bay (72 %), and these proportions were higher than those at sites S4 and S5 in the southern part of Jiaozhou Bay (56 % and 52 %, respectively). Moreover, there was a significant difference in the size distribution of MPs between the dry season and the rainy season (Mann-Whitney U test, $p < 0.05$). The mean and median sizes of AMPs in the dry season were 404.103 ± 596.327 μm and 165.175 μm, respectively, while those in the rainy season were 191.375 ± 259.289 μm and 102.911 μm, respectively (Fig. 4f). The proportion of MPs smaller than 500 μm was higher in the rainy season (93 %) than in the dry season (76 %) (Fig. 4d). Fig. 4e shows that the overall size distribution of AMPs in the dry season was larger than that in the rainy season.

A similar pattern of small particle size MPs predominance was found in other studies of AMPs conducted in different cities, such as Shanghai (70.47 % MPs < 500 μm), Jakarta (87.88 % MPs < 500 μm), Mexico City (63 %–69 % MPs < 500 μm) and Sri Lanka (>50 % MPs < 500 μm) (Jia et al., 2022; Perera et al., 2022; Purwiyanto et al., 2022; Shruti et al., 2022). However, the mean particle size of AMPs in Jiaozhou Bay (331.507 ± 517.323 μm) was lower than that in Shanghai (524.57 ± 619.49 μm) and Sri Lanka (768.63 ± 25.42 μm), and significantly lower than that in Jiaozhou Bay seawater (1290 ± 700 μm), sediment (1200 ± 780 μm) and benthic organisms (1103.4 μm) (Zhang et al., 2023; Zheng et al., 2019). These results may indicate that the main source of MPs in Jiaozhou Bay is the fragmentation and degradation of larger plastic, and the smaller mean particle size reflects a higher degree of weathering. This hypothesis is also in line with the highest proportion of small particle size MPs observed in quarter Q3 (summer), when the high temperature and sunlight exposure accelerated the breakdown of large plastics. Nevertheless, it should be noted that several factors may influence the particle size distribution of the collected AMPs, as indicated by previous studies. These factors include the sampling height, the sampler inlet port sizes, and the laboratory pretreatment procedures. Specifically, MPs with different shapes and sizes have different aerodynamic equivalent diameters, which affect their rates of deposition (Finlay and Darquenne, 2020; Henn, 1996). Fibrous MPs, characterized by larger dimensions, exhibit slower deposition rates and longer residence times in comparison to granular MPs (Bullard et al., 2021). Hence, disparities in the sampling height can influence the obtained MPs' size distribution. Klein et al. (2023) pointed out that studies with notably high fibrous MPs counts were predominantly executed on roofs in large metropolitan areas with heights between 15 and 50 m. In this study, site S5, distinguished by its largest sampling height, manifests the highest proportion of large-diameter MPs among all sites (27 % MPs > 500 μm). This result may illustrate the effect of sampling height on the particle size of MPs. Moreover, the study in Iran showed that a smaller inlet port of the sampler resulted in a smaller overall particle size of MPs (Abbasi

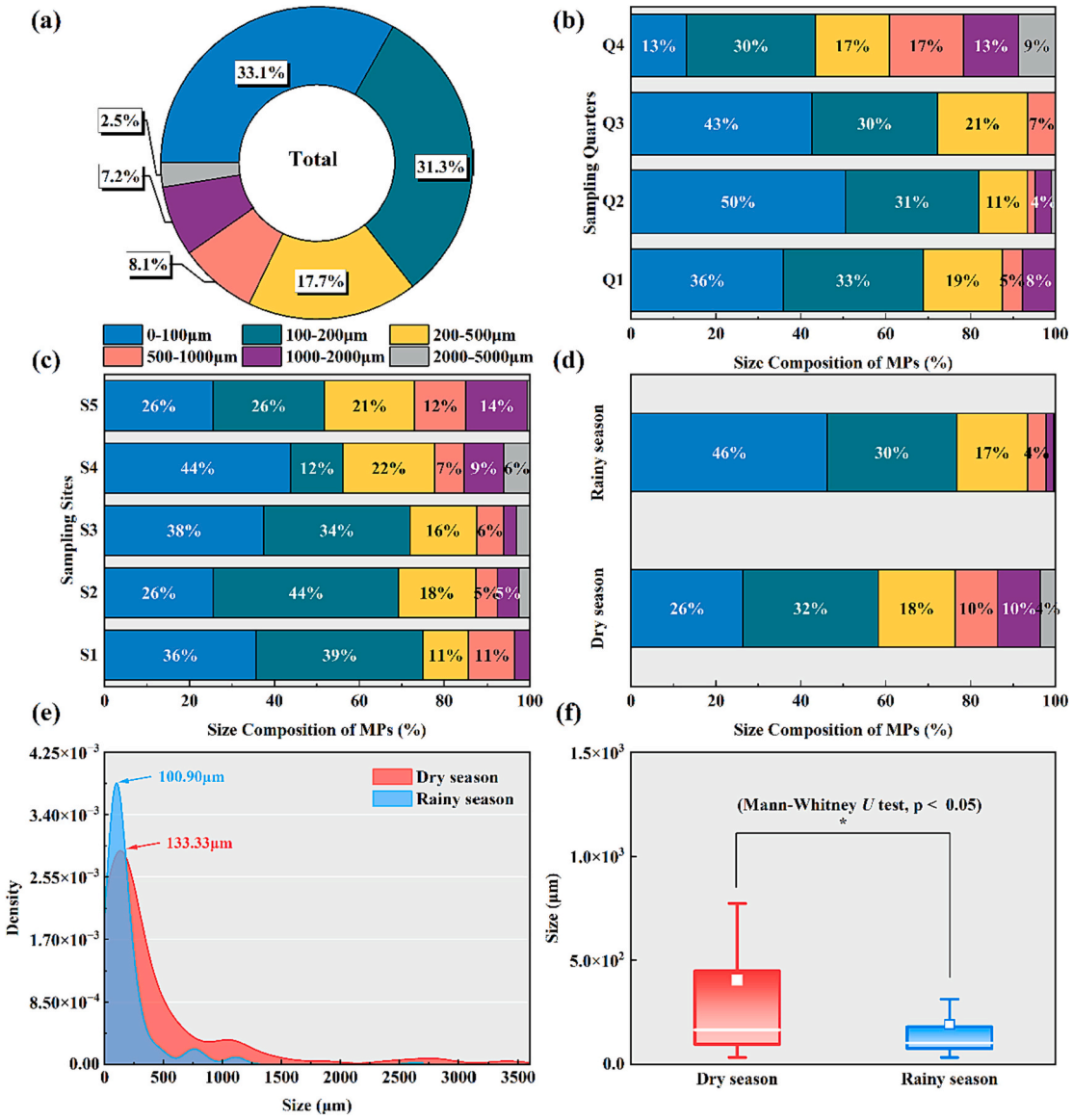

Fig. 4. Proportion of AMPs sizes in Jiaozhou Bay. (a) The percentage of all AMPs sizes. (b) The percentage of AMPs sizes in different quarters. (c) The percentage of AMPs sizes in different sampling sites. (d) The percentage of AMPs sizes in dry and rainy seasons. (e) Size distribution of AMPs in dry and rainy seasons. (f) The average size of AMPs in dry and rainy seasons.

et al., 2019). The study in Jakarta used a stainless-steel sieve with a 200 μm pore size for filtration in the MPs pretreatment, which may cause the loss of MPs below 200 μm (Purwiyanto et al., 2022). Therefore, further research is needed to verify the reason for the smaller particle size of MPs observed in this study.

3.2. Occurrence and abundance of AMPs

We detected MPs at all sampling sites and quarters. To estimate the abundance of MPs, we measured the deposition rate of AMPs. The AMP deposition rate in Jiaozhou Bay ranged from 8.395 to 80.114 items·m^{-2}·d^{-1}, with an average of 46.708 ± 21.316 items·m^{-2}·d^{-1}. The average AMP deposition rates in quarters Q1 to Q4 were 73.247 ± 11.096, 29.063 ± 6.189, 34.14 ± 17.556 and 50.382 ± 12.679 items·m^{-2}·d^{-1}, respectively, with corresponding medians of 80.114, 27.679, 33.580 and 54.763 items·m^{-2}·d^{-1}. The Kruskal-Wallis test revealed significant differences among the quarterly averages ($p < 0.05$) (Fig. 5a). Furthermore, the average AMP deposition rates at sites S1 to S5 were 39.083 ± 14.221, 54.54 ± 19.154, 44.941 ± 19.765, 45.491 ± 27.125, and 49.485 ± 21.085 items·m^{-2}·d^{-1}, respectively, with corresponding medians of 47.150, 46.727, 39.590, 52.233, and 41.614 items·m^{-2}·d^{-1}. However, no significant differences were observed among the site averages (Kruskal-Wallis test) (Fig. 5b). Additionally, the AMP deposition rates in the dry and rainy seasons were 61.563 ± 8.301 items·m^{-2}·d^{-1} and 31.587 ± 7.279 items·m^{-2}·d^{-1}, respectively, with corresponding medians of 58.765 items·m^{-2}·d^{-1} and 36.179 items·m^{-2}·d^{-1}. The Mann-Whitney *U* test indicated that the AMP deposition rate in the dry season was significantly higher than that in the rainy season ($p < 0.05$) (Fig. 5c).

We estimated the mass of MPs entering Jiaozhou Bay through atmospheric deposition by using the formula in Section 2.5 and the density values of different chemical types of MPs (Table S1). The average mass of a single AMP was 1.006 × 10^{-6} g. Based on the mass of AMPs, the deposition rate (items·m^{-2}·d^{-1}), and the water area of Jiaozhou Bay (444 km^2), we can calculate the annual abundance and mass of MPs input into Jiaozhou Bay through atmospheric deposition. The results showed that atmospheric deposition added (7.569 ± 3.455) × 10^{12} items and 7.612 ± 3.474 tons of MPs to Jiaozhou Bay every year.

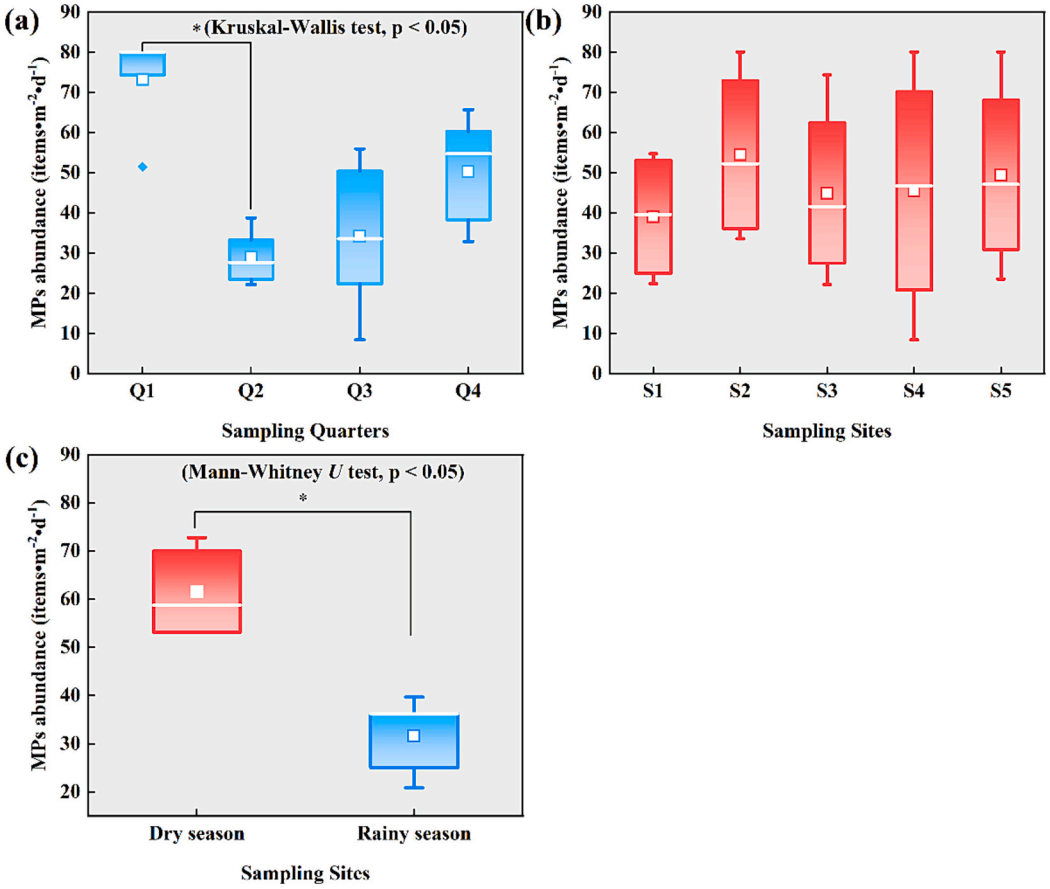

Fig. 5. The deposition rate of AMPs in Jiaozhou Bay during the sampling period. (a) The deposition rate of AMPs in different quarters. (b) The deposition rate of AMPs in different sampling sites. (c) The deposition rate of AMPs types in dry and rainy seasons.

According to previous studies, the total content of MPs in the surface seawater is estimated to be 1.786 ± 0.995 × 10^{10} items (sea area of Jiaozhou Bay: 444 km^2; depth of the surface seawater: 0.5 m) (Liu et al., 2020a). Zheng et al. (2020) and Zhang et al. (2023) reported that the sediment and benthic fauna in Jiaozhou Bay contain 3.71 to 6.06 tons and 36.4 kg of MPs, respectively. Meijer et al. (2021) modeled that Jiaozhou Bay emitted 614.9 tons of plastic per year. These results suggest that atmospheric deposition is a significant source of MPs for the water body of Jiaozhou Bay. Moreover, we observed a similar seasonal variation of AMPs and MPs in surface water and copepods in Jiaozhou Bay, both peaking in Q1 (winter) and Q4 (autumn) and declining in Q2 (spring) and Q3 (summer) (Ouyang et al., 2020; Zheng et al., 2021). Since the MPs entering the ocean through land runoff increased with the precipitation in spring and summer, we inferred that the high abundance of MPs in copepods in autumn and winter might result from the ingestion of AMPs deposited in surface seawater. This finding also provides evidence for the impact of AMPs on marine ecology.

Jiaozhou Bay, which lies within the city of Qingdao, receives MPs from urban sources. To assess the level of AMPs in Jiaozhou Bay, we used passive sampling methods and compared the results with other coastal urban areas that applied the same methods (Table 2). The comparison showed that Jiaozhou Bay had a relatively low abundance of AMPs, only higher than Yantai (40 items·m^{-2}·d^{-1}) and Jakarta (15 ± 13 items·m^{-2}·d^{-1}), but significantly lower than Tianjin (244.9 items·m^{-2}·d^{-1}), Dalian (197.7 items·m^{-2}·d^{-1}), Guangzhou (114 ± 40 items·m^{-2}·d^{-1}), Shanghai (3261.22 ± 2847.99 items·m^{-2}·d^{-1}), Hamburg (275 items·m^{-2}·d^{-1}), London (771 ± 167 items·m^{-2}·d^{-1}), and Ho Chi Minh city (71– 917 items·m^{-2}·d^{-1}).

We attribute this finding to the different environmental characteristics of the sampling sites in different studies. For example, factors such as population density and industrial activity may influence the abundance of MPs, as more people and industries generate more sources of MPs. Cities such as Shanghai (3923 inhabitants/km^2), Hamburg (2453 inhabitants/km^2), London (2976 inhabitants/km^2), and Ho Chi Minh City (4375 inhabitants/km^2) have higher population densities than Qingdao (1110 inhabitants/km^2). On the other hand, Jakarta's Ancol

Table 2
Abundance of the AMPs in different cities.

Sampling area	Sampling method	City type	Abundance	Reference
Yantai, China	Passive sampling	Coastal city	40 items·m^{-2}·d^{-1}	(Zhou et al., 2017)
Tianjin, China	Passive sampling	Coastal city	244.9 items·m^{-2}·d^{-1}	(Tian et al., 2020)
Dalian, China	Passive sampling	Coastal city	197.7 items·m^{-2}·d^{-1}	(Tian et al., 2020)
Guangzhou, China	Passive sampling	Coastal city	114 ± 40 items·m^{-2}·d^{-1}	(Huang et al., 2021)
Shanghai, China	Passive sampling	Coastal city	3261.22 ± 2847.99 items·m^{-2}·d^{-1}	(Jia et al., 2022)
Hamburg, Germany	Passive sampling	Coastal city	275 items·m^{-2}·d^{-1}	(Klein and Fischer, 2019)
London, UK	Passive sampling	Coastal city	771 ± 167 items·m^{-2}·d^{-1}	(Wright et al., 2020)
Ho Chi Minh, Vietnam	Passive sampling	Coastal city	71– 917 items·m^{-2}·d^{-1}	(Truong et al., 2021)
Jakarta, Indonesia	Passive sampling	Coastal city	15 ± 13 items·m^{-2}·d^{-1}	(Purwiyanto et al., 2022)
Qingdao, China	Passive sampling	Coastal city	46.708 ± 21.316 items·m^{-2}·d^{-1}	This research

(99 inhabitants/km^2) and Yantai's population density (452 inhabitants/km^2) are significantly lower. Moreover, since this study was conducted in the urban center and the suburbs at the same time, the average MPs abundance was reduced by the lower MPs abundance in the suburbs, such as the S1 site.

Previous studies have shown that the abundance of AMPs obtained by passive sampling is also influenced by the distance to the coastline, the filter pore size, and the sampling height. Coastal areas have lower AMPs abundance due to the dilution effect of ocean air (Liu et al., 2019). Using filters with large pore size may miss small-sized AMPs during the laboratory analysis (Purwiyanto et al., 2022). Sampling height influences the number of AMPs collected by passive sampling in different ways. Higher sampling sites have less interference from ground obstacles and more exposure to upper-altitude winds that carry distant AMPs. However, lower sampling sites may also increase the capture of ground-originated AMPs. These factors result in inconsistent findings on the relationship between sampling height and AMPs abundance in previous studies. Liu et al. (2019) found that the abundance of AMPs decreased as the sampling altitude increased. Truong et al. (2021) reported a positive correlation between sampling elevation and AMP deposition rates. In this study, the sites with the highest sampling altitude (S2 and S5) had the largest MPs deposition rates. However, the differences among all the sampling sites were not statistically significant, which could be attributed to the mixing effects of convective airflows.

3.3. Influence factors and sources

Several factors influence the abundance and distribution of AMPs, such as precipitation and wind. Researchers have suggested that precipitation accelerates the deposition of AMPs (Dris et al., 2016). Rainfall erodes and deposits many MPs on the ground, increasing their abundance and decreasing their particle size in wet weather compared to dry weather (Jia et al., 2022). Allen et al. (2019) found a positive correlation between MPs deposition and precipitation intensity and frequency, but not duration. Roblin et al. (2020) indicated that relative humidity and rainfall affect the wet deposition of MPs. Dong et al. (2021) reported that rainfall intensity had a significant positive correlation with MPs deposition flux, but rainfall amount did not. Wind also affects the deposition of MPs, but in complex and diverse ways. Wright et al. (2020) observed correlations between MPs abundance and wind direction and speed. Allen et al. (2019) showed that the frequency of winds with wind speed >1 m/s had a positive correlation with MPs deposition flux.Liu et al. (2019), Browne et al. (2010) argued that wind significantly influenced the spatial distribution of suspended AMPs, resulting in higher abundance in the downwind direction. Szewc et al. (2021) examined the relationship between AMPs and various meteorological factors and discovered that wind speed affected the deposition rate of MPs by influencing their dry deposition. Purwiyanto et al. (2022) claimed that wind lifted AMPs particles and prevented them from settling.

As Fig. 6a shows, we examined the precipitation status during the sampling period. The Jiaozhou Bay area experienced the lowest precipitation in quarter Q1, followed by an increase in Q2 and Q3, a peak in Q3, and a decrease in Q4. Out of the 365 days of the sampling period, 286 days had no precipitation, 68 days had light rain (0–10 mm rainfall within 24 h), 5 days had moderate rain (10–25 mm rainfall within 24 h), and 6 days had heavy rain (>25 mm rainfall within 24 h). Moderate and heavy rain accounted for only 1.37 % and 1.64 % of the year, respectively. The rainy season had significantly smaller AMPs particle size in Jiaozhou Bay than the dry season, indicating the effect of precipitation on AMPs deposition (Fig. 4e and f). However, we found no significant correlation between precipitation and AMPs abundance. We suggest that one possible reason is the low amount and intensity of precipitation in the Jiaozhou Bay area, which reduces the impact of precipitation on AMPs deposition. Other factors, such as wind, temperature, and plastic production, may also influence AMPs deposition. Therefore, seasonal change in AMPs deposition does not reflect the effect of precipitation. Moreover, since we sampled quarterly in this study, the lower sampling frequency may have affected the correlation analysis between precipitation and AMPs abundance.

We examined the annual and seasonal wind direction and wind speed in the Jiaozhou Bay area (Fig. 6a, b and Fig. S2). To identify the source of AMPs in Jiaozhou Bay, we used the Hysplit model (web version) to conduct a 24-h backward trajectory analysis for site S1 from December 2018 to December 2019 (Fig. 7). We performed the analysis at heights of 10 m, 100 m and 500 m, starting at 8 am on the 5th of each month. We also compared the atmospheric motion trajectories between different sites (S1 to S5) on March 4, June 4, September 3, and December 5 by analyzing their 24-h backward trajectories (Figs. S3 to S7). The results of wind direction and wind speed analysis show that the annual wind direction in Jiaozhou Bay is mainly north-northwest and south-southeast, with higher wind speed in Q1 and Q4. The wind direction in Q1 and Q4 is mainly northwest, while in Q2 and Q3 it is mainly

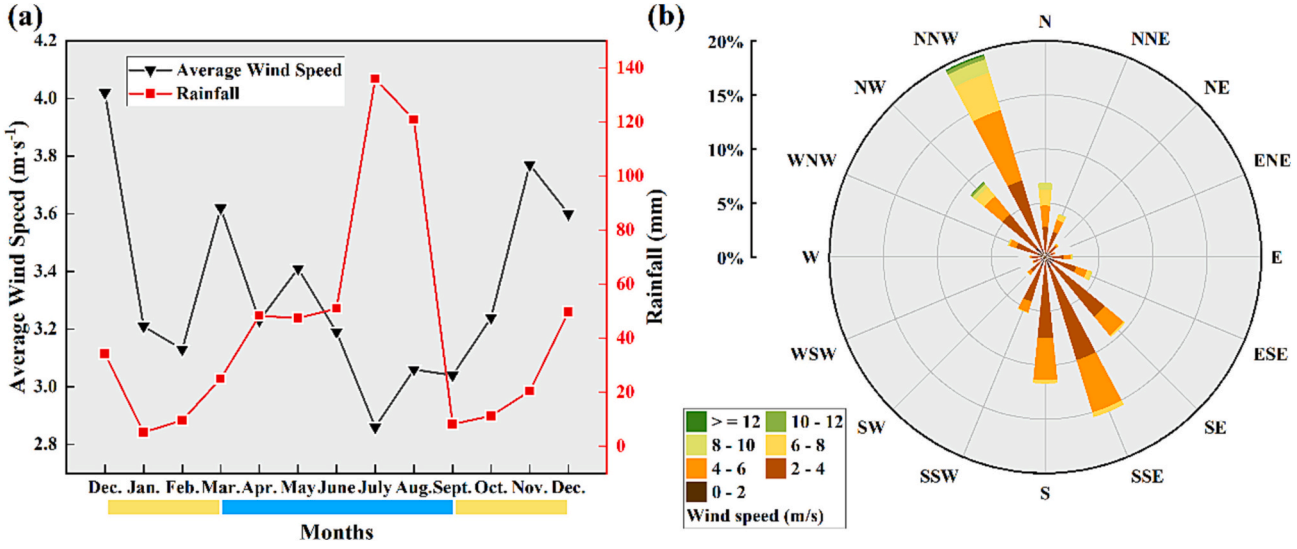

Fig. 6. The weather condition in Jiaozhou Bay during sampling period. (a) The rainfall (red square dash line), and average wind speed (black triangle dash line) during the rainy (blue line) and dry (yellow line) seasons. (b) The wind rose diagram depicts the predominant wind direction and speed in Jiaozhou Bay. (For interpretation of the references to colour in this figure legend, the reader is referred to the web version of this article.)

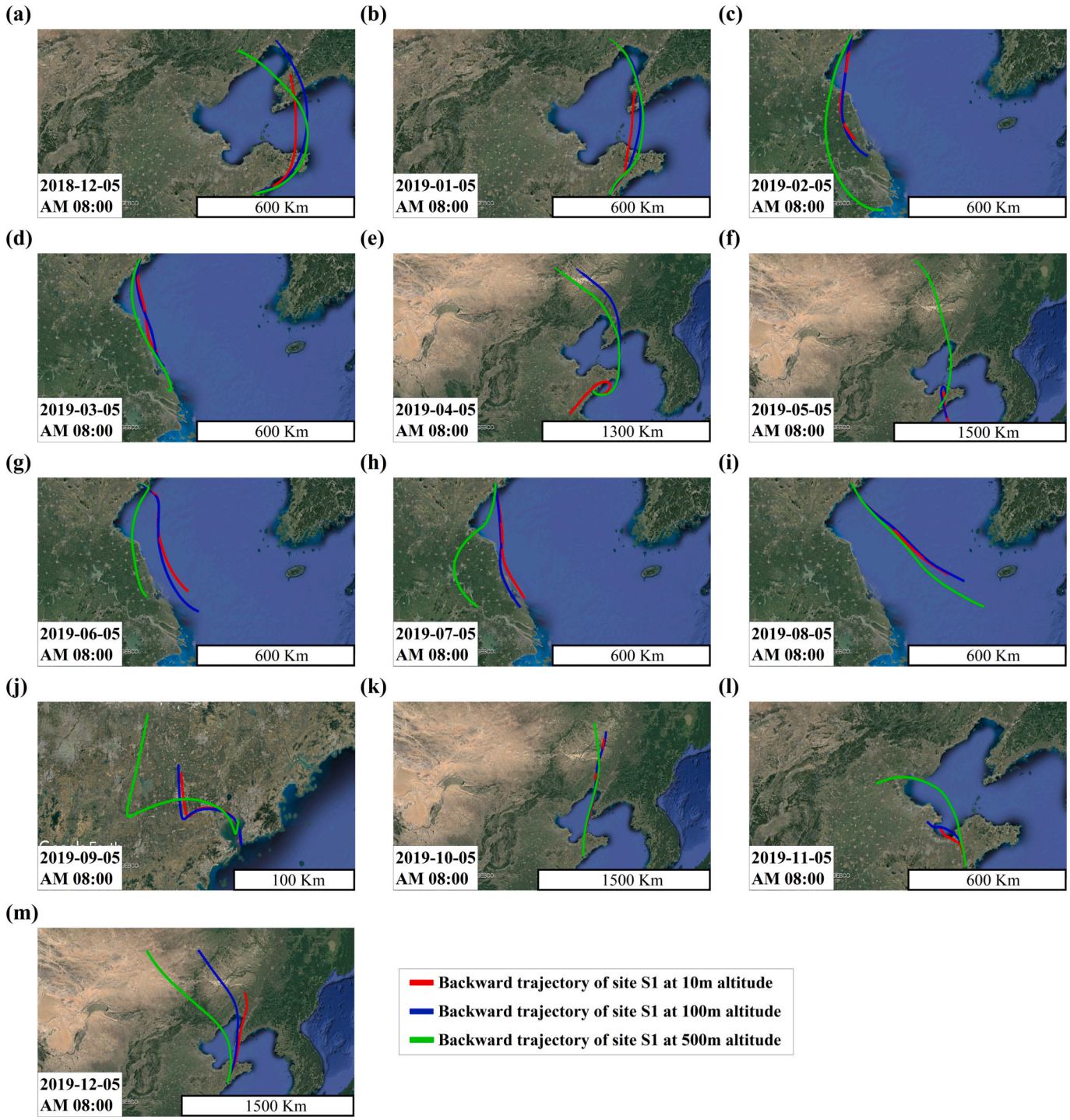

Fig. 7. The 24-h backward trajectory of site S1 during the sampling period. (a) to (m) represent the backward trajectory in different months. The bottom left corner of the image shows the time point at which the backward trajectory analysis begins, and the bottom right corner of the image shows the display distance corresponding to the length in the image. The red line represents the backward trajectory at 10 m altitude; the blue line represents the backward trajectory at 100 m altitude; and the green line represents the backward trajectory at 500 m altitude. (For interpretation of the references to colour in this figure legend, the reader is referred to the web version of this article.)

southeast. The backward trajectory analysis shows that the airflow at site S1 mainly originates from the urban agglomeration of Shandong Peninsula in the north of Jiaozhou Bay in Q1 and Q4, and from the Yellow Sea in the southeast of Jiaozhou Bay in Q2 and Q3. The results are consistent with the wind direction. Different sites have similar atmospheric trajectories, originating from the same area. Therefore, we suggest that the wind plays a dominant role in the distribution of AMPs in Jiaozhou Bay. In Q1 and Q4, the northwest wind carries the MPs particles produced by the urban agglomeration in the northern part of Jiaozhou Bay to Jiaozhou Bay, resulting in higher AMPs abundance. In Q2, the southeast wind blows from the Yellow Sea to the land, reducing the transport of MPs. In Q3, the increased precipitation raises the average humidity of the air, leading to more AMPs deposition. Finally, the quarterly distribution of AMPs abundance follows a pattern of Q1 > Q4 > Q3 > Q2.

To investigate the influence of human activities on the abundance of

AMPs, we examined the correlation between the human activity indicators of the administrative regions where the sampling sites were located and the AMPs deposition (Table S2 and Fig. S8). The correlation analysis showed a weak relationship between various human activity variables and AMPs. This could be attributed to the homogenization of AMPs due to the short distance among the sampling sites and the long-range transport of AMPs.

4. Conclusion

This study reveals that Jiaozhou Bay has a lower abundance of AMPs than other bay regions, mainly consisting of fragmented and fibrous MPs with PET, PE, and cellulose as the main constituents. The distribution of AMPs varies temporally and spatially, and differs between dry and wet deposition. Seasonal analysis indicates that the abundance of MPs follows the pattern of winter (Q1) > autumn (Q4) > summer (Q3) > spring (Q2). Monsoons and precipitation affect the deposition of AMPs, with monsoons having a dominant role. Regional analysis indicates that there are significant differences among regions, but no clear correlation with population density and human activities. In future work, we will conduct high-frequency sampling of AMPs, and collect more detailed data on the surrounding environment to verify the relationship between various environmental factors and the distribution of MPs. Moreover, we suggest that future assessments of AMPs exposure risk should consider the monsoon changes in the assessment area, as well as the sources and atmospheric transport of MPs from surrounding areas, to provide a more comprehensive evaluation of the ecological risk posed by AMPs.

Supplementary data to this article can be found online at https://doi.org/10.1016/j.marpolbul.2023.115568.

CRediT authorship contribution statement

Chenhao Zhao: Methodology, Formal analysis, Visualization, Writing – original draft. **Junhua Liang:** Conceptualization, Methodology, Validation, Investigation. **Mingliang Zhu:** Methodology, Investigation, Resources. **Shan Zheng:** Conceptualization, Methodology, Data curation. **Yongfang Zhao:** Conceptualization, Methodology, Data curation. **Xiaoxia Sun:** Conceptualization, Methodology, Writing – review & editing, Supervision, Project administration, Funding acquisition.

Declaration of competing interest

The authors declare that they have no known competing financial interests or personal relationships that could have appeared to influence the work reported in this paper.

Data availability

Data will be made available on request.

Acknowledgement

This work was supported by the National Natural Science Foundation of China (No. U2006206), the National Natural Science Foundation of China (No. 42006118), the Strategic Priority Research Program of the Chinese Academy of Sciences (No. XDA23050303), the International Science Partnership Program of the Chinese Academy of Sciences (No. 133137KYSB20200002), the International Science Partnership Program of the Chinese Academy of Sciences (No. 121311KYSB20190029), and the Taishan Scholars Project (to SUN Song).

References

Abbasi, S., Keshavarzi, B., Moore, F., Turner, A., Kelly, F.J., Dominguez, A.O., Jaafarzadeh, N., 2019. Distribution and potential health impacts of microplastics and microrubbers in air and street dusts from Asaluyeh County, Iran. Environ. Pollut. 244, 153–164. https://doi.org/10.1016/j.envpol.2018.10.039.

Allen, S., Allen, D., Phoenix, V.R., Le Roux, G., Durántez Jiménez, P., Simonneau, A., Galop, D., 2019. Atmospheric transport and deposition of microplastics in a remote mountain catchment. Nat. Geosci. 12 (5), 339–344. https://doi.org/10.1038/s41561-019-0335-5.

Allen, S., Allen, D., Baladima, F., Phoenix, V.R., Thomas, J.L., Le Roux, G., Sonke, J.E., 2021. Evidence of free tropospheric and long-range transport of microplastic at Pic du Midi Observatory. Nat. Commun. 12 (1), 7242. https://doi.org/10.1038/s41467-021-27454-7.

Allen, D., Allen, S., Abbasi, S., Baker, A., Bergmann, M., Brahney, J., Wright, S., 2022. Microplastics and nanoplastics in the marine-atmosphere environment. Nat. Rev. Earth Environ. 3 (6), 393–405. https://doi.org/10.1038/s43017-022-00292-x.

Andrady, A.L., 2011. Microplastics in the marine environment. Mar. Pollut. Bull. 62 (8), 1596–1605. https://doi.org/10.1016/j.marpolbul.2011.05.030.

Bergmann, M., Mützel, S., Primpke, S., Tekman, M.B., Trachsel, J., Gerdts, G., 2019. White and wonderful? Microplastics prevail in snow from the Alps to the Arctic. Sci. Adv. 5 (8) https://doi.org/10.1126/sciadv.aax1157.

Bonifazi, G., Fiore, L., Pelosi, C., Serranti, S., 2023. Evaluation of plastic packaging waste degradation in seawater and simulated solar radiation by spectroscopic techniques. In: Polymer Degradation and Stability, p. 207. https://doi.org/10.1016/j.polymdegradstab. 2022.110215.

Browne, M.A., Galloway, T.S., Thompson, R.C., 2010. Spatial patterns of plastic debris along estuarine shorelines. Environ. Sci. Technol. 44 (9), 3404–3409. https://doi.org/10.1021/es903784e.

Bullard, J.E., Ockelford, A., O'Brien, P., McKenna Neuman, C., 2021. Preferential transport of microplastics by wind. Atmos. Environ. 245 https://doi.org/10.1016/j.atmosenv.2020.118038.

Cai, L., Wang, J., Peng, J., Tan, Z., Zhan, Z., Tan, X., Chen, Q., 2017. Characteristic of microplastics in the atmospheric fallout from Dongguan city, China: preliminary research and first evidence. Environ. Sci. Pollut. Res. Int. 24 (32), 24928–24935. https://doi.org/10.1007/s11356-017-0116-x.

Chen, J., 2015. Chapter 4- synthetic textile fibers: regenerated cellulose fibers. In: Sinclair, R. (Ed.), Textiles and Fashion. Woodhead Publishing, pp. 79–95.

Chu, J., Zhou, Y., Cai, Y., Wang, X., Li, C., Liu, Q., 2023. Flows and waste reduction strategies of PE, PP, and PET plastics under plastic limit order in China. Resour. Conserv. Recycl. 188, 106668. https://doi.org/10.1016/j.resconrec.2022.106668.

Cole, M., Lindeque, P., Halsband, C., Galloway, T.S., 2011. Microplastics as contaminants in the marine environment: a review. Mar. Pollut. Bull. 62 (12), 2588–2597. https://doi.org/10.1016/j.marpolbul.2011.09.025.

Dhakal, H.N., Ismail, S.O., 2021. 1- Introduction to composite materials. In: Dhakal, H. N., Ismail, S.O. (Eds.), Sustainable Composites for Lightweight Applications. Woodhead Publishing, pp. 1–16.

Ding, J., Li, J., Sun, C., Jiang, F., He, C., Zhang, M., Ding, N.X., 2020. An examination of the occurrence and potential risks of microplastics across various shellfish. Sci. Total Environ. 739, 139887. https://doi.org/10.1016/j.scitotenv.2020.139887.

Dong, H., Wang, L., Wang, X., Xu, L., Chen, M., Gong, P., Wang, C., 2021. Microplastics in a remote Lake Basin of the Tibetan plateau: impacts of atmospheric transport and glacial melting. Environ. Sci. Technol. 55 (19), 12951–12960. https://doi.org/10.1021/acs.est.1c03227.

Dris, R., Gasperi, J., Rocher, V., Saad, M., Renault, N., Tassin, B., 2015. Microplastic contamination in an urban area: a case study in Greater Paris. Environ. Chem. 12 (5), 592–599. https://doi.org/10.1071/en14167.

Dris, R., Gasperi, J., Saad, M., Mirande, C., Tassin, B., 2016. Synthetic fibers in atmospheric fallout: a source of microplastics in the environment? Mar. Pollut. Bull. 104 (1), 290–293. https://doi.org/10.1016/j.marpolbul.2016.01.006.

Evangeliou, N., Grythe, H., Klimont, Z., Heyes, C., Eckhardt, S., Lopez-Aparicio, S., Stohl, A., 2020. Atmospheric transport is a major pathway of microplastics to remote regions. Nat. Commun. 11 (1), 3381. https://doi.org/10.1038/s41467-020-17201-9.

Fendall, L.S., Sewell, M.A., 2009. Contributing to marine pollution by washing your face: microplastics in facial cleansers. Mar. Pollut. Bull. 58 (8), 1225–1228. https://doi.org/10.1016/j.marpolbul.2009.04.025.

Ferrero, L., Scibetta, L., Markuszewski, P., Mazurkiewicz, M., Drozdowska, V., Makuch, P., Bolzacchini, E., 2022. Airborne and marine microplastics from an oceanographic survey at the Baltic Sea: an emerging role of air-sea interaction? Sci. Total Environ. 824, 153709. https://doi.org/10.1016/j.scitotenv.2022.153709.

Finlay, W.H., Darquenne, C., 2020. Particle size distributions. J. Aerosol Med. Pulm. Drug Deliv. 33 (4), 178–180. https://doi.org/10.1089/jamp.2020.29028.whf.

Guo, X., Wang, J., 2021. Projecting the sorption capacity of heavy metal ions onto microplastics in global aquatic environments using artificial neural networks. J. Hazard. Mater. 402, 123709. https://doi.org/10.1016/j.jhazmat.2020.123709.

Hahladakis, J.N., Velis, C.A., Weber, R., Iacovidou, E., Purnell, P., 2018. An overview of chemical additives present in plastics: migration, release, fate and environmental impact during their use, disposal and recycling. J. Hazard. Mater. 344, 179–199. https://doi.org/10.1016/j.jhazmat.2017.10.014.

Henn, A.R., 1996. Calculation of the stokes and aerodynamic equivalent diameters of a short reinforcing fiber. Part. Part. Syst. Charact. 13 (4), 249–253. https://doi.org/10.1002/ppsc.19960130407.

Huang, Y., He, T., Yan, M., Yang, L., Gong, H., Wang, W., Wang, J., 2021. Atmospheric transport and deposition of microplastics in a subtropical urban environment. J. Hazard. Mater. 416, 126168. https://doi.org/10.1016/j.jhazmat.2021.126168.

Huang, X., Chen, Y., Meng, Y., Liu, G., Yang, M., 2022. Are we ignoring the role of urban forests in intercepting atmospheric microplastics? J. Hazard. Mater. 436, 129096. https://doi.org/10.1016/j.jhazmat.2022.129096.

Hüffer, T., Praetorius, A., Wagner, S., von der Kammer, F., Hofmann, T., 2017. Microplastic exposure assessment in aquatic environments: learning from similarities

and differences to engineered nanoparticles. Environ. Sci. Technol. 51 (5), 2499–2507. https://doi.org/10.1021/acs.est.6b04054.
Jia, Q., Duan, Y., Han, X., Sun, X., Munyaneza, J., Ma, J., Xiu, G., 2022. Atmospheric deposition of microplastics in the megalopolis (Shanghai) during rainy season: characteristics, influence factors, and source. Sci. Total Environ. 847, 157609. https://doi.org/10.1016/j.scitotenv.2022.157609.
Jiao, J., Chen, G., Yang, Z., Li, Z., Hu, H., 2022. Microplastics in surface waters and floodplain sediments of the Dagu River in the Jiaodong Peninsula, China. J. Ocean Univ. China 21 (6), 1538–1548. https://doi.org/10.1007/s11802-022-5211-z.
Klein, M., Fischer, E.K., 2019. Microplastic abundance in atmospheric deposition within the metropolitan area of Hamburg, Germany. Sci. Total Environ. 685, 96–103. https://doi.org/10.1016/j.scitotenv.2019.05.405.
Klein, M., Bechtel, B., Brecht, T., Fischer, E.K., 2023. Spatial distribution of atmospheric microplastics in bulk-deposition of urban and rural environments – a one-year follow-up study in northern Germany. Sci. Total Environ. 901, 165923. https://doi.org/10.1016/j.scitotenv.2023.165923.
Kutralam-Muniasamy, G., Shruti, V.C., Pérez-Guevara, F., Roy, P.D., 2023a. Microplastic diagnostics in humans: "the 3Ps" Progress, problems, and prospects. Sci. Total Environ. 856, 159164. https://doi.org/10.1016/j.scitotenv.2022.159164.
Kutralam-Muniasamy, G., Shruti, V.C., Pérez-Guevara, F., Roy, P.D., 2023b. Microplastic diagnostics in humans: "the 3Ps" Progress, problems, and prospects. Sci. Total Environ. 856 https://doi.org/10.1016/j.scitotenv.2022.159164.
Li, P., Pu, S., Li, Z., & Wang, H. (2020). Coastline change monitoring of Jiaozhou Bay from multi-source SAR and optical remote sensing images since 2000. Geomatics and Information Science of Wuhan University, 45(9), 1485–1492. doi:10.13203/j.whugis20180483.
Liu, K., Wang, X., Fang, T., Xu, P., Zhu, L., Li, D., 2019. Source and potential risk assessment of suspended atmospheric microplastics in Shanghai. Sci. Total Environ. 675, 462–471. https://doi.org/10.1016/j.scitotenv.2019.04.110.
Liu, Y., Li, Z., Jalon-Rojas, I., Wang, X.H., Fredj, E., Zhang, D., Li, X., 2020a. Assessing the potential risk and relationship between microplastics and phthalates in surface seawater of a heavily human-impacted metropolitan bay in northern China. Ecotoxicol. Environ. Saf. 204, 111067. https://doi.org/10.1016/j.ecoenv.2020.111067.
Liu, T., Zhao, Y., Zhu, M., Liang, J., Zheng, S., Sun, X., 2020b. Seasonal variation of micro- and meso-plastics in the seawater of Jiaozhou Bay, the Yellow Sea. Mar. Pollut. Bull. 152, 110922. https://doi.org/10.1016/j.marpolbul.2020.110922.
Liu, P., Shao, L., Li, Y., Jones, T., Cao, Y., Yang, C.-X., BéruBé, K., 2022. Microplastic atmospheric dustfall pollution in urban environment: evidence from the types, distribution, and probable sources in Beijing, China. Sci. Total Environ. 838 https://doi.org/10.1016/j.scitotenv.2022.155989.
Long, X., Fu, T.-M., Yang, X., Tang, Y., Zheng, Y., Zhu, L., Li, B., 2022. Efficient atmospheric transport of microplastics over Asia and adjacent oceans. Environ. Sci. Technol. 56 (10), 6243–6252. https://doi.org/10.1021/acs.est.1c07825.
Mbachu, O., Jenkins, G., Pratt, C., Kaparaju, P., 2020. A new contaminant superhighway? A review of sources, measurement techniques and fate of atmospheric microplastics. Water Air Soil Pollut. 231 (2) https://doi.org/10.1007/s11270-020-4459-4.
Meijer, L.J.J., van Emmerik, T., van der Ent, R., Schmidt, C., Lebreton, L., 2021. More than 1000 rivers account for 80% of global riverine plastic emissions into the ocean. Sci. Adv. 7 (18), eaaz5803. https://doi.org/10.1126/sciadv.aaz5803.
O'Brine, T., Thompson, R.C., 2010. Degradation of plastic carrier bags in the marine environment. Mar. Pollut. Bull. 60 (12), 2279–2283. https://doi.org/10.1016/j.marpolbul.2010.08.005.
Ouyang, W., Zhang, Y., Wang, L., Barcelo, D., Wang, Y., Lin, C., 2020. Seasonal relevance of agricultural diffuse pollutant with microplastic in the bay. J. Hazard. Mater. 396, 122602. https://doi.org/10.1016/j.jhazmat.2020.122602.
Pastorino, P., Nocita, A., Ciccotelli, V., Zaccaroni, A., Anselmi, S., Giugliano, R., Prearo, M., 2021. Health risk assessment of potentially toxic elements, persistence of NDL-PCB, PAHs, and microplastics in the translocated edible freshwater Sinotaia quadrata (Gasteropoda, Viviparidae): a case study from the Arno River basin (Central Italy). Expo. Health 13 (4), 583–596. https://doi.org/10.1007/s12403-021-00404-w.
Perera, K., Ziajahromi, S., Bengtson Nash, S., Manage, P.M., Leusch, F.D.L., 2022. Airborne microplastics in indoor and outdoor environments of a developing country in South Asia: abundance, distribution, morphology, and possible sources. Environ. Sci. Technol. 56 (23), 16676–16685. https://doi.org/10.1021/acs.est.2c05885.
Pironti, C., Ricciardi, M., Motta, O., Miele, Y., Proto, A., Montano, L., 2021. Microplastics in the environment: intake through the food web, human exposure and toxicological effects. Toxics 9 (9). https://doi.org/10.3390/toxics9090224.
Purwiyanto, A.I.S., Prartono, T., Riani, E., Naulita, Y., Cordova, M.R., Koropitan, A.F., 2022. The deposition of atmospheric microplastics in Jakarta-Indonesia: the coastal urban area. Mar. Pollut. Bull. 174, 113195. https://doi.org/10.1016/j.marpolbul.2021.113195.
Qingdao Municipal Statistics Bureau, 2020. Qingdao Statistical Yearbook 2020. Retrieved from. http://qdtj.qingdao.gov.cn/tongjisj/tjsj_tjnj/tjnj_2020/202204/P020220414508740435062.pdf.
Rahman, A., Sarkar, A., Yadav, O.P., Achari, G., Slobodnik, J., 2021. Potential human health risks due to environmental exposure to nano- and microplastics and knowledge gaps: a scoping review. Sci. Total Environ. 757, 143872. https://doi.org/10.1016/j.scitotenv.2020.143872.
Raspisaniye Pogodi Ltd, 2023. rp5.ru. Retrieved from. https://rp5.ru/Weather_in_the_world.
Ratner, B.D., 2012. 9.21- polymeric implants. In: Matyjaszewski, K., Möller, M. (Eds.), Polymer Science: A Comprehensive Reference. Elsevier, Amsterdam, pp. 397–411.
Roblin, B., Ryan, M., Vreugdenhil, A., Aherne, J., 2020. Ambient atmospheric deposition of anthropogenic microfibers and microplastics on the western periphery of Europe (Ireland). Environ. Sci. Technol. 54 (18), 11100–11108. https://doi.org/10.1021/acs.est.0c04000.
Rochman, C.M., 2018. Microplastics research—from sink to source. Science 360 (6384), 28–29. https://doi.org/10.1126/science.aar7734.
de Sá, L.C., Oliveira, M., Ribeiro, F., Rocha, T.L., Futter, M.N., 2018. Studies of the effects of microplastics on aquatic organisms: what do we know and where should we focus our efforts in the future? Sci. Total Environ. 645, 1029–1039. https://doi.org/10.1016/j.scitotenv.2018.07.207.
Shruti, V.C., Kutralam-Muniasamy, G., Pérez-Guevara, F., Roy, P.D., Martínez, I.E., 2022. Occurrence and characteristics of atmospheric microplastics in Mexico City. Sci. Total Environ. 847 https://doi.org/10.1016/j.scitotenv.2022.157601.
Suteja, Y., Atmadipoera, A.S., Riani, E., Nurjaya, I.W., Nugroho, D., Cordova, M.R., 2021. Spatial and temporal distribution of microplastic in surface water of tropical estuary: case study in Benoa Bay, Bali, Indonesia. Mar. Pollut. Bull. 163, 111979. https://doi.org/10.1016/j.marpolbul.2021.111979.
Szewc, K., Graca, B., Dołęga, A., 2021. Atmospheric deposition of microplastics in the coastal zone: characteristics and relationship with meteorological factors. Sci. Total Environ. 761, 143272. https://doi.org/10.1016/j.scitotenv.2020.143272.
Tian, Y., Tu, C., Zhou, Q., Zhang, C., Li, L., Tian, C., Luo, Y., 2020. The temporal and spatial distribution and surface morphology of atmospheric microplastics around the Bohai Sea. Acta Sci. Circumst. 40 (4), 1401–1409.
Truong, T.-N.-S., Strady, E., Kieu-Le, T.-C., Tran, Q.-V., Le, T.-M.-T., Thuong, Q.-T., 2021. Microplastic in atmospheric fallouts of a developing southeast Asian megacity under tropical climate. Chemosphere 272, 129874. https://doi.org/10.1016/j.chemosphere.2021.129874.
Wang, W., Gao, H., Jin, S., Li, R., Na, G., 2019. The ecotoxicological effects of microplastics on aquatic food web, from primary producer to human: a review. Ecotoxicol. Environ. Saf. 173, 110–117. https://doi.org/10.1016/j.ecoenv.2019.01.113.
Wang, X., Wei, N., Liu, K., Zhu, L., Li, C., Zong, C., Li, D., 2022. Exponential decrease of airborne microplastics: from megacity to open ocean. Sci. Total Environ. 849, 157702. https://doi.org/10.1016/j.scitotenv.2022.157702.
Wang, H., Zhu, J., He, Y., Wang, J., Zeng, N., Zhan, X., 2023. Photoaging process and mechanism of four commonly commercial microplastics. J. Hazard. Mater. 451, 131151. https://doi.org/10.1016/j.jhazmat.2023.131151.
Wright, S.L., Ulke, J., Font, A., Chan, K.L.A., Kelly, F.J., 2020. Atmospheric microplastic deposition in an urban environment and an evaluation of transport. Environ. Int. 136 https://doi.org/10.1016/j.envint.2019.105411.
Xu, A., Shi, M., Xing, X., Su, Y., Li, X., Liu, W., Qi, S., 2022. Status and prospects of atmospheric microplastics: a review of methods, occurrence, composition, source and health risks. Environ. Pollut. 303, 119173. https://doi.org/10.1016/j.envpol.2022.119173.
Xuan, L., Xiao, L., Huang, R., 2023. The geno-toxicological impacts of microplastic (MP) exposure on health: mechanistic pathways and research trends from a Chinese perspective. In: Environmental Science: Processes & Impacts. https://doi.org/10.1039/D2EM00301E.
Yukioka, S., Tanaka, S., Nabetani, Y., Suzuki, Y., Ushijima, T., Fujii, S., Singh, S., 2020. Occurrence and characteristics of microplastics in surface road dust in Kusatsu (Japan), Da Nang (Vietnam), and Kathmandu (Nepal). Environ. Pollut. 256 https://doi.org/10.1016/j.envpol.2019.113447.
Zhang, K., Zheng, S., Liang, J., Zhao, Y., Li, Q., Zhu, M., Sun, X., 2023. Microplastic load of benthic fauna in Jiaozhou Bay, China. Environ. Pollut. 320, 121073. https://doi.org/10.1016/j.envpol.2023.121073.
Zheng, Y., Li, J., Cao, W., Liu, X., Jiang, F., Ding, J., Sun, C., 2019. Distribution characteristics of microplastics in the seawater and sediment: a case study in Jiaozhou Bay, China. Sci. Total Environ. 674, 27–35. https://doi.org/10.1016/j.scitotenv.2019.04.008.
Zheng, Y., Li, J., Cao, W., Jiang, F., Zhao, C., Ding, H., Sun, C., 2020. Vertical distribution of microplastics in bay sediment reflecting effects of sedimentation dynamics and anthropogenic activities. Mar. Pollut. Bull. 152, 110885. https://doi.org/10.1016/j.marpolbul.2020.110885.
Zheng, S., Zhao, Y., Liu, T., Liang, J., Zhu, M., Sun, X., 2021. Seasonal characteristics of microplastics ingested by copepods in Jiaozhou Bay, the Yellow Sea. Sci. Total Environ. 776, 145936. https://doi.org/10.1016/j.scitotenv.2021.145936.
Zhou, Q., Tian, C., Luo, Y., 2017. Various forms and deposition fluxes of microplastics identified in the coastal urban atmosphere. Chin. Sci. Bull. 62 (33), 3902–3909 (Retrieved from <Go to ISI>://CSCD:6145725).